

## Chapter 13

# Fixed points, and how to get them

Cycles. Is there anything they can't do?

— Mason Porter, channeling Homer Simpson

**H**AVING SET UP the dynamical context, we now turn to the key and unavoidable numerical task in this subject; we must search for the solutions  $(x, T)$ ,  $x \in \mathbb{R}^d$ ,  $T \in \mathbb{R}$  satisfying the *periodic orbit condition*

$$f^{t+T}(x) = f^t(x), \quad T > 0 \quad (13.1)$$

for a given flow or map.

In chapters 18 and 19 we will establish that spectra of evolution operators can be extracted from periodic orbit sums:

$$\sum (\text{spectral eigenvalues}) = \sum (\text{periodic orbits}) .$$

Hence, periodic orbits are the necessary ingredient for evaluation of the spectra of evolution operators. We need to know what periodic orbits can exist, and the symbolic dynamics developed so far is an invaluable tool toward this end.

Sadly, searching for periodic orbits will never become as popular as a week on Côte d'Azur, or publishing yet another log-log plot in *Phys. Rev. Letters*. This chapter is intended as a hands-on guide to extracting periodic orbits, and should be skipped on first reading - you can return to it whenever the need for finding actual cycles arises. A serious cyclist will want to also learn about the variational methods to find cycles, chapter 29. They are particularly useful when little is known about the topology of a flow, such as in high-dimensional periodic orbit searches.

chapter 29



fast track:  
chapter 14, p. 290

A *prime* cycle  $p$  of period  $T_p$  is a single traversal of the periodic orbit, so our task will be to find a periodic point  $x \in \mathcal{M}_p$  and the shortest time  $T_p$  for which (13.1) has a solution. A periodic point of a flow  $f^t$  crossing a Poincaré section  $n$  times is a fixed point of  $P^n$ , the  $n$ th iterate of  $P$ , the return map (3.1); hence, we shall refer to all cycles as “fixed points” in this chapter. By cyclic invariance, Floquet multipliers and the period of the cycle are independent of the choice of the initial point, so it will suffice to solve (13.1) at a single periodic point.

section 5.2

If the cycle is an attracting limit cycle with a sizable basin of attraction, it can be found by integrating the flow for a sufficiently long time. If the cycle is unstable, simple integration forward in time will not reveal it, and the methods to be described here need to be deployed. In essence, any method for finding a cycle is based on devising a new dynamical system which possesses the same cycle, but for which this cycle is attractive. Beyond that, there is a great freedom in constructing such systems, and many different methods are used in practice.

Due to the exponential divergence of nearby trajectories in chaotic dynamical systems, fixed point searches based on direct solutions of the fixed-point condition (13.1) as an initial value problem can be numerically very unstable. Methods that start with initial guesses for a number of points along the cycle, such as the multipoint shooting method described here in sect. 13.3, and the variational methods of chapter 29, are considerably more robust and safer.

chapter 29

A prerequisite for any exhaustive cycle search is a good understanding of the topology of the flow: a preliminary step to any serious periodic orbit calculation is preparing a list of all distinct admissible prime periodic symbol sequences, such as the list given in table 15.1. The relations between the temporal symbol sequences and the spatial layout of the topologically distinct regions of the state space discussed in chapters 11 and 12 should enable us to guess the location of a series of periodic points along a cycle. Armed with such an informed guess we proceed to improve it by methods such as Newton-Raphson iteration; we show how this works by applying Newton method to 1- and  $d$ -dimensional maps. But first, where are the cycles?

### 13.1 Where are the cycles?

Q: What if you choose a really bad initial condition and it doesn't converge? A: Well then you only have yourself to blame.

— T.D. Lee

The simplest and conceptually easiest setting for guessing where the cycles are is the case of planar billiards. The Maupertuis principle of least action here dictates that the physical trajectories extremize the length of an approximate orbit that visits a desired sequence of boundary bounces.

**Example 13.1 Periodic orbits of billiards.** Consider how this works for 3-disk pinball game of sect. 12.5. . Label the three disks by 1, 2 and 3, and associate to section 12.5 section 1.4

trajectory an itinerary, a sequence of labels indicating the order in which the disks are visited, as in figure 3.8. Given the itinerary, you can construct a guess trajectory by taking a point on the boundary of each disk in the sequence, and connecting them by straight lines. Imagine that this is a rubber band wrapped through 3 rings, and shake the band until it shrinks into the physical trajectory, the rubber band of shortest length.

Extremization of a cycle length requires variation of  $n$  bounce positions  $s_i$ . The computational problem is to find the extremum values of cycle length  $L(s)$  where  $s = (s_1, \dots, s_n)$ , a task that we postpone to sect. 29.3. As an example, the short periods and stabilities of 3-disk cycles computed this way are listed table 29.3, and some examples are plotted in figure 3.8. It's a no brainer, and millions of such cycles have been computed.

If we were only so lucky. Real life finds us staring at something like Yang-Mills or Navier-Stokes equations, utterly clueless. What to do?

One, there is always mindless computation. In practice one might be satisfied with any rampaging robot that finds “the most important” cycles. The ergodic explorations of recurrences to which we turn next sometimes perform admirably well.

### 13.1.1 Cycles from long time series

Two wrongs don't make a right, but three lefts do.  
—Appliance guru

(L. Rondoni and P. Cvitanović)

The equilibria and periodic orbits (with the exception of sinks and stable limit cycles) are never seen in simulations and experiments because they are unstable. Nevertheless, one does observe close passes to the least unstable equilibria and periodic orbits, as in figure 13.1. Ergodic exploration by long-time trajectories (or long-lived transients, in case of strange repellers) can uncover state space regions of low velocity, or finite time recurrences. In addition, such trajectories preferentially sample the natural measure of the ‘turbulent’ flow, and by initiating searches within the state space concentrations of natural measure bias the search toward the dynamically important invariant solutions.

The search consists of following a long trajectory in state space, and looking for close returns of the trajectory to itself, see figure 13.1. Whenever the trajectory almost closes in a loop (within a given tolerance), another point close to this near miss of a cycle can be taken as an initial condition. Supplemented by a Newton routine described below, a sequence of improved initial conditions may indeed rapidly lead to closing a cycle. The method preferentially finds the least unstable orbits, while missing the more unstable ones that contribute little to the cycle expansions.

This blind search is seriously flawed: in contrast to the 3-disk example 13.1, it is not systematic, it gives no insight into organization of the ergodic sets, and

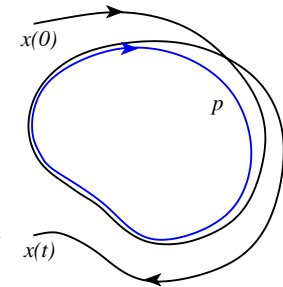


Figure 13.1: An ergodic trajectory can shadow an unstable periodic orbit  $p$  for a finite time.

can easily miss very important cycles. Foundations to a systematic exploration of ergodic state space are laid in chapters 11 and 12, but are a bit of work to implement.

### 13.1.2 Cycles found by thinking

Thinking is extra price.  
—Dicho Colombiano

A systematic charting out of state space starts out by a hunt for equilibrium points. If the equations of motion are a finite set of ODEs, setting the velocity field  $v(x)$  in (2.6) to zero reduces search for equilibria to a search for zeros of a set of algebraic equations. We should be able, in principle, to enumerate and determine all real and complex zeros in such cases, e.g. the Lorenz example 2.2 and the Rössler example 2.3. If the equations of motion and the boundary conditions are invariant under some symmetry, some equilibria can be determined by symmetry considerations: if a function is e.g. antisymmetric, it must vanish at origin, e.g. the Lorenz  $EQ_0 = (0, 0, 0)$  equilibrium.

As to other equilibria: if you have no better idea, create a state space grid, about 50  $x_k$  across  $\mathcal{M}$  in each dimension, and compute the velocity field  $v_k = v(x_k)$  at each grid point; a few million  $v_k$  values are easily stored. Plot  $x_k$  for which  $|v_k|^2 < \epsilon$ ,  $\epsilon \ll |v_{max}|^2$  but sufficiently large that a few thousand  $x_k$  are plotted. If the velocity field varies smoothly across the state space, the regions  $|v_k|^2 < \epsilon$  isolate the (candidate) equilibria. Start a Newton iteration with the smallest  $|v_k|^2$  point within each region. Barring exceptionally fast variations in  $v(x)$  this should yield all equilibrium points.

For ODEs equilibria are fixed points of algebraic sets of equations, but steady states of PDEs such as the Navier-Stokes flow are themselves solutions of ODEs or PDEs, and much harder to determine.

Equilibria—by definition—do not move, so they cannot be “turbulent.” What makes them dynamically important are their stable/unstable manifolds. A chaotic trajectory can be thought of as a sequence of near visitations of equilibria. Typi-

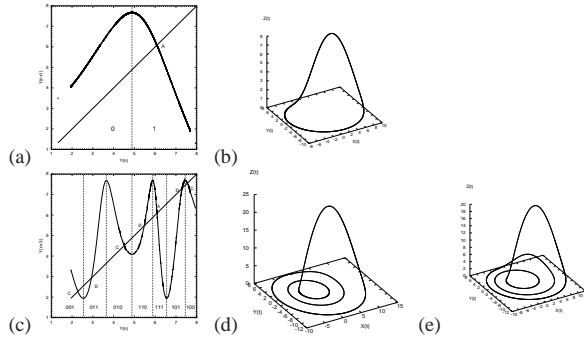


**Figure 13.2:** (a) The  $y \rightarrow P_1(y, z)$  return map for the  $x = 0, y > 0$  Poincaré section of the Rössler flow figure 2.6. (b) The  $\bar{1}$ -cycle found by taking the fixed point  $y_{k+n} = y_k$  together with the fixed point of the  $z \rightarrow z$  return map (not shown) as an initial guess  $(0, y^{(0)}, z^{(0)})$  for the Newton-Raphson search. (c) The third iterate,  $y_{k+3} = P_1^3(y_k, z_k)$ , of the Poincaré return map (3.1) together with the corresponding plot for  $z_{k+3} = P_2^3(y_k, z_k)$ , is used to pick initial guesses for the Newton-Raphson searches for the two 3-cycles: (d) the  $\bar{001}$  cycle, and (e) the  $\bar{011}$  cycle. (G. Simon)

cally such neighborhoods have many stable, contracting directions and a handful of unstable directions. Our strategy will be to generalize the billiard Poincaré section maps  $P_{S_{n+1} \leftarrow S_n}$  of example 3.9 to maps from a section of the unstable manifold of equilibrium  $S_n$  to the section of unstable manifold of equilibrium  $S_{n+1}$ , and thus reduce the continuous time flow to a sequence of maps. These Poincaré section maps do double duty, providing us both with an exact representation of dynamics in terms of maps, and with a covering symbolic dynamics.

We showed in the Lorenz flow example 11.4 how to reduce the 3-dimensional Lorenz flow to a 1-dimensional return map. In the Rössler flow example 2.3 we sketched the attractor by running a long chaotic trajectory, and noting that the attractor is very thin, but that otherwise the return maps that we plotted were disquieting – figure 3.3 did not appear to be a 1-to-1 map. In the next example we show how to use such information to locate cycles approximately. In the remainder of this chapter and in chapter 29 we shall learn how to turn such guesses into highly accurate cycles.

**Example 13.2 Rössler attractor.** We run a long simulation of the Rössler flow  $f^t$ , plot a Poincaré section, as in figure 3.2, and extract the corresponding Poincaré return map  $P$ , as in figure 3.3. Luck is with us, since figure 13.2(a) return map  $y \rightarrow P_1(y, z)$  is quite reminiscent of a parabola, we take the unimodal map symbolic dynamics, sect. 11.3, as our guess for the covering dynamics. Strictly speaking, the attractor is “fractal,” but for all practical purposes the return map is 1-dimensional; your printer will need a resolution better than  $10^{14}$  dots per inch to even begin resolving its structure.

Periodic points of a prime cycle  $p$  of cycle length  $n_p$  for the  $x = 0, y > 0$  Poincaré section of the Rössler flow figure 2.6 are fixed points  $(y, z) = P^{n_p}(y, z)$  of the  $n$ th Poincaré return map.

Using the fixed point  $y_{k+1} = y_k$  in figure 13.2(a) together with the simultaneous fixed point of the  $z \rightarrow P_1(y, z)$  return map (not shown) as a starting guess  $(0, y^{(0)}, z^{(0)})$  for the Newton-Raphson search for the cycle  $p$  with symbolic dynamics label  $\bar{1}$ , we find the cycle figure 13.2(b) with the Poincaré section point  $(0, y_p, z_p)$ , period  $T_p$ , expanding, marginal, contracting Floquet multipliers  $(\Lambda_{p,e}, \Lambda_{p,m}, \Lambda_{p,c})$ , and the corresponding Lyapunov exponents  $(\lambda_{p,e}, \lambda_{p,m}, \lambda_{p,c})$ :

exercise 13.10

$$\begin{aligned} \bar{1}\text{-cycle:} \quad (x, y, z) &= (0, 6.09176832, 1.2997319) \\ T_1 &= 5.88108845586 \\ (\Lambda_{1,e}, \Lambda_{1,m}, \Lambda_{1,c}) &= (-2.40395353, 1 + 10^{-14}, -1.29 \times 10^{-14}) \\ (\lambda_{1,e}, \lambda_{1,m}, \lambda_{1,c}) &= (0.149141556, 10^{-14}, -5.44). \end{aligned} \tag{13.2}$$

The Newton-Raphson method that we used is described in sect. 13.4.

As an example of a search for longer cycles, we use  $y_{k+3} = P_1^3(y_k, z_k)$ , the third iterate of the Poincaré return map (3.1) plotted in figure 13.2(c), together with a corresponding plot for  $z_{k+3} = P_2^3(y_k, z_k)$ , to pick starting guesses for the Newton-Raphson searches for the two 3-cycles plotted in figure 13.2(d), (e). For a listing of the short cycles of the Rössler flow, consult exercise 13.10.

The numerical evidence suggests (though a proof is lacking) that all cycles that comprise the strange attractor of the Rössler flow are hyperbolic, each with an expanding eigenvalue  $|\Lambda_e| > 1$ , a contracting eigenvalue  $|\Lambda_c| < 1$ , and a marginal eigenvalue  $|\Lambda_m| = 1$  corresponding to displacements along the direction of the flow.

For the Rössler flow the contracting eigenvalues turn out to be insanely contracting, a factor of  $e^{-32}$  per one par-course of the attractor, so their numerical determination is quite difficult. Fortunately, they are irrelevant; for all practical purposes the strange attractor of the Rössler flow is 1-dimensional, a very good realization of a horseshoe template. (G. Simon and P. Cvitanović)

## 13.2 One-dimensional maps

(F. Christiansen)

### 13.2.1 Inverse iteration

Let us first consider a very simple method to find the unstable cycles of a 1-dimensional map such as the logistic map. Unstable cycles of 1 – dimensional maps are attracting cycles of the inverse map. The inverse map is not single-valued, so at each backward iteration we have a choice of branch to make. By choosing the branch according to the symbolic dynamics of the cycle we are trying to find, we will automatically converge to the desired cycle. The rate of convergence is given by the stability of the cycle, i.e., the convergence is exponentially fast. Figure 13.3 shows such a path to the  $\bar{01}$ -cycle of the logistic map.

exercise 13.13

The method of inverse iteration is fine for finding cycles for 1-d maps and some 2-dimensional systems such as the repeller of exercise 13.13. It is not particularly fast, however, especially if the inverse map is not known analytically. It also completely fails for higher dimensional systems where we have both stable and unstable directions. Inverse iteration will exchange these, but we will still be left with both stable and unstable directions. The best strategy is to directly attack the problem of finding solutions of  $f^T(x) = x$ .

**Figure 13.3:** The inverse time path to the  $\overline{01}$ -cycle of the logistic map  $f(x) = 4x(1 - x)$  from an initial guess of  $x = 0.2$ . At each inverse iteration we chose the 0 (respectively 1) branch.

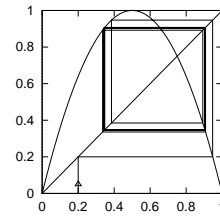
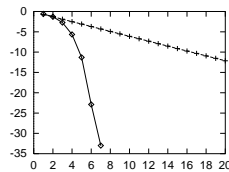


**Figure 13.4:** Convergence of Newton method ( $\diamond$ ) vs. inverse iteration ( $+$ ). The error after  $n$  iterations searching for the  $\overline{01}$ -cycle of the logistic map  $f(x) = 4x(1 - x)$  with an initial starting guess of  $x_1 = 0.2, x_2 = 0.8$ . The y-axis is  $\log_{10}$  of the error. The difference between the exponential convergence of the inverse iteration method and the super-exponential convergence of Newton method is dramatic.



### 13.2.2 Newton method

Newton method for determining a zero  $x^*$  of a function  $F(x)$  of one variable is based on a linearization around a starting guess  $x_0$ :

$$F(x) \approx F(x_0) + F'(x_0)(x - x_0). \tag{13.3}$$

An approximate solution  $x_1$  of  $F(x) = 0$  is

$$x_1 = x_0 - F(x_0)/F'(x_0). \tag{13.4}$$

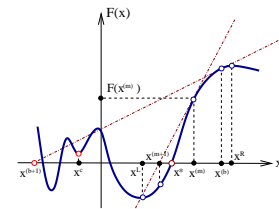
The approximate solution can then be used as a new starting guess in an iterative process. A fixed point of a map  $f$  is a solution to  $F(x) = x - f(x) = 0$ . We determine  $x$  by iterating

$$\begin{aligned} x_m &= g(x_{m-1}) = x_{m-1} - F(x_{m-1})/F'(x_{m-1}) \\ &= x_{m-1} - \frac{1}{1 - f'(x_{m-1})}(x_{m-1} - f(x_{m-1})). \end{aligned} \tag{13.5}$$

Provided that the fixed point is not marginally stable,  $f'(x) \neq 1$  at the fixed point  $x$ , a fixed point of  $f$  is a super-stable fixed point of the Newton-Raphson map  $g$ ,  $g'(x) = 0$ , and with a sufficiently good initial guess, the Newton-Raphson iteration will converge super-exponentially fast.

To illustrate the efficiency of Newton method we compare it to the inverse iteration method in figure 13.4. Newton method wins hands down: the number of significant digits of the accuracy of the  $x$  estimate typically doubles with each iteration.

**Figure 13.5:** Newton method: bad initial guess  $x^{(b)}$  leads to the Newton estimate  $x^{(b+1)}$  far away from the desired zero of  $F(x)$ . Sequence  $\dots, x^{(m)}, x^{(m+1)}, \dots$ , starting with a good guess converges super-exponentially to  $x^*$ . The method diverges if it iterates into the basin of attraction of a local minimum  $x^*$ .



In order to avoid jumping too far from the desired  $x^*$  (see figure 13.5), one often initiates the search by the *damped Newton method*,

$$\Delta x_m = x_{m+1} - x_m = -\frac{F(x_m)}{F'(x_m)} \Delta \tau, \quad 0 < \Delta \tau \leq 1,$$

takes small  $\Delta \tau$  steps at the beginning, reinstating to the full  $\Delta \tau = 1$  jumps only when sufficiently close to the desired  $x^*$ .

### 13.3 Multipoint shooting method

(F. Christiansen)

Periodic orbits of length  $n$  are fixed points of  $f^n$  so in principle we could use the simple Newton method described above to find them. However, this is not an optimal strategy. The function  $f^n$  oscillates wildly, with as many as  $2^n$  or more closely spaced fixed points, and finding a specific periodic point, such as one with a given symbolic sequence, requires a *very* good starting guess. For binary symbolic dynamics we must expect to improve the accuracy of our initial guesses by at least a factor of  $2^n$  to find orbits of length  $n$ . A better alternative is the *multipoint* or *multiple shooting method*. While it might very hard to give a precise initial guess for a long periodic orbit, if our guesses are informed by a good state space partition, a rough guess for each point along the desired trajectory might suffice, as for the individual short trajectory segments the errors have no time to explode exponentially. And, indeed, in chapter 11 we have developed a qualitative theory of how these cycle points are laid out topologically.

A cycle of length  $n$  is a zero of the  $n$ -dimensional vector function  $F$ :

$$F(x) = F \begin{pmatrix} x_1 \\ x_2 \\ \vdots \\ x_n \end{pmatrix} = \begin{pmatrix} x_1 - f(x_n) \\ x_2 - f(x_1) \\ \vdots \\ x_n - f(x_{n-1}) \end{pmatrix}.$$

The relationship between the temporal symbol sequences and the spatial layout of the topologically distinct regions of state space discussed in chapter 11 enable

us to guess the location of a series of periodic points along a cycle. Armed with such informed initial guesses, we can initiate a Newton-Raphson iteration. The iteration in Newton's method now takes the form

$$\frac{d}{dx}F(x)(x' - x) = -F(x), \tag{13.6}$$

where  $\frac{d}{dx}F(x)$  is an  $[n \times n]$  matrix:

$$\frac{d}{dx}F(x) = \begin{pmatrix} 1 & & & & -f'(x_n) \\ -f'(x_1) & 1 & & & \\ & \dots & & & \\ & & 1 & & \\ & & & \dots & \\ & & & & 1 & \\ & & & -f'(x_{n-1}) & & 1 \end{pmatrix}. \tag{13.7}$$

This matrix can easily be inverted numerically by first eliminating the elements below the diagonal. This creates non-zero elements in the  $n$ th column. We eliminate these and are done.

**Example 13.3 Newton inversion for a 3-cycle.** Let us illustrate how this works step by step for a 3-cycle. The initial setup for a Newton step is:

$$\begin{pmatrix} 1 & 0 & -f'(x_3) \\ -f'(x_1) & 1 & 0 \\ 0 & -f'(x_2) & 1 \end{pmatrix} \begin{pmatrix} \Delta x_1 \\ \Delta x_2 \\ \Delta x_3 \end{pmatrix} = - \begin{pmatrix} F_1 \\ F_2 \\ F_3 \end{pmatrix},$$

where  $\Delta x_i = x'_i - x_i$  is the correction to our initial guess  $x_i$ , and  $F_i = x_i - f(x_{i-1})$  is the error at  $i$ th periodic point. Eliminate the sub-diagonal elements by adding  $f'(x_1)$  times the first row to the second row, then adding  $f'(x_2)$  times the second row to the third row:

$$\begin{pmatrix} 1 & 0 & -f'(x_3) \\ 0 & 1 & -f'(x_1)f'(x_3) \\ 0 & 0 & 1 - f'(x_2)f'(x_1)f'(x_3) \end{pmatrix} \begin{pmatrix} \Delta x_1 \\ \Delta x_2 \\ \Delta x_3 \end{pmatrix} = - \begin{pmatrix} F_1 \\ F_2 + f'(x_1)F_1 \\ F_3 + f'(x_2)F_2 + f'(x_2)f'(x_1)F_1 \end{pmatrix}.$$

The next step is to invert the last element in the diagonal, i.e., divide the third row by  $1 - f'(x_2)f'(x_1)f'(x_3)$ . If this element is zero at the periodic orbit this step cannot work. As  $f'(x_2)f'(x_1)f'(x_3)$  represents the stability of the cycle (when the Newton iteration has converged), this is not a good method to find marginally stable cycles. We now have

$$\begin{pmatrix} 1 & 0 & -f'(x_3) \\ 0 & 1 & -f'(x_1)f'(x_3) \\ 0 & 0 & 1 \end{pmatrix} \begin{pmatrix} \Delta x_1 \\ \Delta x_2 \\ \Delta x_3 \end{pmatrix} = - \begin{pmatrix} F_1 \\ F_2 + f'(x_1)F_1 \\ \frac{F_3 + f'(x_2)F_2 + f'(x_2)f'(x_1)F_1}{1 - f'(x_2)f'(x_1)f'(x_3)} \end{pmatrix}.$$

Finally we add  $f'(x_3)$  times the third row to the first row and  $f'(x_1)f'(x_3)$  times the third row to the second row. The left hand side matrix is now the unit matrix, and the right hand side is an explicit formula for the corrections to our initial guess. With this, we have gone through one Newton iteration.

When one sets up Newton iteration on a computer, it is not necessary to write the left hand side as a matrix. All one needs is a vector containing the  $f'(x_i)$ 's and a vector containing the  $n$ 'th column, i.e., the cumulative product of the  $f'(x_i)$ 's and a vector containing the right hand side. After iteration the vector containing the right hand side is the correction to the initial guess.

exercise 13.1

### 13.3.1 $d$ -dimensional maps



Armed with clever initial guesses from a system's symbolic dynamics, we can easily extend the Newton-Raphson iteration method to  $d$ -dimensional maps. In this case  $f'(x_i)$  is a  $[d \times d]$  matrix, and  $\frac{d}{dx}F(x)$  is an  $[nd \times nd]$  matrix. In each of the steps above, we are then manipulating  $d$  rows of the left-hand-side matrix. (Remember that matrices do not commute - always multiply from the left.) In inverting the  $n$ th element of the diagonal we are inverting a  $[d \times d]$  matrix  $(1 - \prod f'(x_i))$  which can be done as long as none of the eigenvalues of  $\prod f'(x_i)$  equals 1, i.e., if the cycle has no marginally stable eigen-directions.

**Example 13.4 Newton method for time delay maps.** Some  $d$ -dimensional maps (such as the Hénon map (3.17)) can be written as 1-dimensional time delay maps of the form

$$f(x_i) = f(x_{i-1}, x_{i-2}, \dots, x_{i-d}). \tag{13.8}$$

In this case,  $\frac{d}{dx}F(x)$  is an  $[n \times n]$  matrix as in the case of usual 1-dimensional maps but with non-zero matrix elements on  $d$  off-diagonals.

## 13.4 Flows

(R. Paškauskas and P. Cvitanović)

For a continuous time flow the periodic orbit the Floquet multiplier (5.16) along the flow direction always equals unity; the separation of any two points along a cycle remains unchanged after a completion of the cycle. More unit Floquet multipliers arise if the flow satisfies conservation laws, such as the symplectic invariance for Hamiltonian flows, or the dynamics is equivariant under a continuous symmetry transformation.

section 5.2.1

section 10.3

Let us apply the Newton method of (13.4) to search for periodic orbits with unit Floquet multipliers, starting with the case of a *continuous time flow*. Assume that the periodic orbit condition (13.1) holds for  $x + \Delta x$  and  $T + \Delta t$ , with the initial guesses  $x$  and  $T$  close to the desired solution, i.e., with  $|\Delta x|, \Delta t$  small. The Newton setup (13.4)

$$\begin{aligned} 0 &= x + \Delta x - f^{T+\Delta t}(x + \Delta x) \\ &\approx x - f^T(x) + (1 - J(x)) \cdot \Delta x - v(f^T(x))\Delta t \end{aligned} \tag{13.9}$$

suffers from two shortcomings. First, we now need to solve not only for the periodic point  $x$ , but for the period  $T$  as well. Second, the marginal, unit Floquet multiplier (5.16) along the flow direction (arising from the time-translation invariance of a periodic orbit) renders the factor  $(1 - J)$  in (13.5) non-invertible: if  $x$  is close to the solution,  $f^T(x) \approx x$ , then  $J(x) \cdot v(x) = v(f^T(x)) \approx v(x)$ . If  $\Delta x$  is parallel to the velocity vector, the derivative term  $(1 - J) \cdot \Delta x \approx 0$ , and it becomes harder to invert  $(1 - J)$  as the iterations approach the solution.

As a periodic orbit  $p$  is a 1-dimensional set of points invariant under dynamics, Newton guess is not improved by picking  $\Delta x$  such that the new point lies on the orbit of the initial one, so we need to constrain the variation  $\Delta x$  to directions transverse to the flow, by requiring, for example, that

$$v(x) \cdot \Delta x = 0. \quad (13.10)$$

Combining this constraint with the variational condition (13.9) we obtain a Newton setup for flows, best displayed in the matrix form:

$$\begin{pmatrix} 1 - J(x) & v(x) \\ v(x) & 0 \end{pmatrix} \begin{pmatrix} \Delta x \\ \Delta t \end{pmatrix} = - \begin{pmatrix} x - f(x) \\ 0 \end{pmatrix} \quad (13.11)$$

This illustrates the general strategy for determining periodic orbits in presence of continuous symmetries - for each symmetry, break the invariance by a constraint, and compute the value of the corresponding continuous parameter (here the period  $T$ ) by iterating the enlarged set of Newton equations. Constraining the variations to transverse ones thus fixes both of Newton's shortcomings: it breaks the time-translation invariance, and the period  $T$  can be read off once the fixed point has been found (hence we omit the superscript in  $f^T$  for the remainder of this discussion).

More generally, the Poincaré surface of section technique of sect. 3.1 turns the periodic orbit search into a fixed point search on a suitably defined surface of section, with a neighboring point variation  $\Delta x$  with respect to a reference point  $x$  constrained to *stay* on the surface manifold (3.2),

$$U(x + \Delta x) = U(x) = 0. \quad (13.12)$$

The price to pay are constraints imposed by the section: in order to *stay* on the surface, arbitrary variation  $\Delta x$  is not allowed.

**Example 13.5 A hyperplane Poincaré section.** *Let us for the sake of simplicity assume that the Poincaré surface of section is a (hyper)-plane, i.e., it is given by the linear condition (3.6)*

$$(x - x_0) \cdot \hat{n} = 0, \quad (13.13)$$

where  $\hat{n}$  is a vector normal to the Poincaré section and  $x_0$  is any point in the Poincaré section. The Newton setup is then (derived as (13.11))

$$\begin{pmatrix} 1 - J & v(x) \\ \hat{n} & 0 \end{pmatrix} \begin{pmatrix} x' - x \\ \Delta t \end{pmatrix} = \begin{pmatrix} -F(x) \\ 0 \end{pmatrix}. \quad (13.14)$$

The last row in this equation ensures that  $x$  will be in the surface of section, and the addition of  $v(x)\Delta t$ , a small vector along the direction of the flow, ensures that such an  $x$  can be found, at least if  $x$  is sufficiently close to a fixed point of  $f$ .

To illustrate that the addition of the extra constraint resolves the problem of  $(1 - J)$  non-invertibility, we consider the particularly simple example of a 3-d flow with the  $(x, y, 0)$ -plane as the Poincaré section,  $a = (0, 0, 1)$ . Let all trajectories cross the Poincaré section perpendicularly, so that  $v = (0, 0, v_z)$ , which means that the marginally stable direction is also perpendicular to the Poincaré section. Furthermore, let the unstable direction be parallel to the  $x$ -axis and the stable direction be parallel to the  $y$ -axis. The Newton setup is now

$$\begin{pmatrix} 1 - \Lambda_u & 0 & 0 & 0 \\ 0 & 1 - \Lambda_s & 0 & 0 \\ 0 & 0 & 0 & v_z \\ 0 & 0 & 0 & 1 \end{pmatrix} \begin{pmatrix} \delta_x \\ \delta_y \\ \delta_z \\ \delta\tau \end{pmatrix} = \begin{pmatrix} -F_x \\ -F_y \\ -F_z \\ 0 \end{pmatrix}. \quad (13.15)$$

If one considers only the upper-left  $[3 \times 3]$  matrix (which we started out with, prior to adding the constraint (13.13)) then this matrix is not invertible and the equation does not have a unique solution. However, the full  $[4 \times 4]$  matrix is invertible, as  $\det(\cdot) = -v_z \det(1 - M_\perp)$ , where  $M_\perp$  is the  $[2 \times 2]$  monodromy matrix for a surface of section transverse to the orbit (see sect. 5.3). (F. Christiansen)

### 13.4.1 Cost function

It pays to think in terms of a *cost* (or *error*) function  $I(\Delta x) = (x + \Delta x - f(x + \Delta x))^2 / 2$ . Periodic orbit condition (13.1) corresponds both to a zero of  $I(\Delta x)$ , and of its first  $\Delta x$  variation. Expand  $I(\Delta x)$  to the second order in  $\Delta x$ ,  $\tilde{I} \approx \tilde{\Delta x}^2 / 2 + (x - f(x)) \cdot \tilde{\Delta x} + (x - f(x))^2 / 2$ , where  $\tilde{\Delta x} = (1 - J(x))\Delta x$ . To find an extremum, we set the derivative with respect to  $\tilde{\Delta x}$  to zero. As the term  $(x - f(x))^2 / 2$  is a constant under  $\Delta x$  variation, let us define an unconstrained *cost function*

$$I_0(\tilde{\Delta x}) = \frac{1}{2} \tilde{\Delta x} \cdot \tilde{\Delta x} + (x - f(x)) \cdot \tilde{\Delta x}, \quad (13.16)$$

Setting the derivative of this function

$$\frac{\partial I_0(\tilde{\Delta x})}{\partial \tilde{\Delta x}} = \tilde{\Delta x} + x - f(x) = (1 - J(x)) \cdot \Delta x + x - f(x) \quad (13.17)$$

to zero recovers the Newton setup (13.4)

Next, we need to enforce the constraint that curbs the directions in which  $\Delta x$  can point. Lagrange multipliers come to help.



covariance matrix  $Q_a$  with a (linearized) deterministic ‘forecast’  $x_k \rightarrow x_{k+1}$ . This is the essential step in implementing data assimilation algorithms by means of a Kalman filter.

An honest calculation requires an honest error estimate. If you are computing a large set of periodic orbits  $p$ , list  $D_p$  along with  $T_p$  and other properties of cycles.

## Résumé

There is no general computational algorithm that is guaranteed to find all solutions (up to a given period  $T_{\max}$ ) to the periodic orbit condition

$$f^{t+T}(x) = f^t(x), \quad T > 0$$

for a general flow or mapping. Due to the exponential divergence of nearby trajectories in chaotic dynamical systems, direct solution of the periodic orbit condition can be numerically very unstable.

A prerequisite for a systematic and complete cycle search is a good (but hard to come by) understanding of the topology of the flow. Usually one starts by - possibly analytic - determination of the equilibria of the flow. Their locations, stabilities, stability eigenvectors and invariant manifolds offer skeletal information about the topology of the flow. The next step is numerical long-time evolution of “typical” trajectories of the dynamical system under investigation. Such numerical experiments build up the “natural measure” and reveal which regions are most frequently visited. Periodic orbit searches can then be initialized by taking nearly recurring orbit segments and deforming them into closed orbits. With a sufficiently good initial guess, the Newton-Raphson formula

$$\begin{pmatrix} 1 - J & v(x) \\ a & 0 \end{pmatrix} \begin{pmatrix} \delta x \\ \delta T \end{pmatrix} = \begin{pmatrix} f(x) - x \\ 0 \end{pmatrix}$$

yields improved estimate  $x' = x + \delta x$ ,  $T' = T + \delta T$ . Iteration then yields the period  $T$  and the location of a periodic point  $x_p$  in the Poincaré section  $(x_p - x_0) \cdot a = 0$ , where  $a$  is a vector normal to the Poincaré section at  $x_0$ .

The problem one faces with high-dimensional flows is that their topology is hard to visualize, and that even with a decent starting guess for a point on a periodic orbit, methods like the Newton-Raphson method are likely to fail. Methods that start with initial guesses for a number of points along the cycle, such as the multipoint shooting method of sect. 13.3, are more robust. Relaxation (or variational) methods take this strategy to its logical extreme, and start by a guess of not a few points along a periodic orbit, but a guess of the entire orbit. Just as these methods are intimately related to variational principles and path integrals, we postpone their introduction until chapter 29.

## Commentary

**Remark 13.1** Close recurrence searches. For low-dimensional maps of flows (for high-dimensional flows, forget about it) picking initial guesses for periodic orbits from close recurrences of a long ergodic trajectory seems like an obvious idea. Nevertheless, ref. [13.1] is frequently cited. Such methods have been deployed by many, among them G. Tanner, L. Rondoni, G. Morris, C.P. Dettmann, and R.L. Davidchack [25.2, 20.14, 20.15, 13.11, 13.12] (see also sect. 20.5). Sometimes one can determine most of the admissible itineraries and their weights without working too hard, but method comes with no guarantee.

**Remark 13.2** Piecewise linear maps. The Lozi map (3.19) is linear, and hundred of thousands of cycles can easily be computed by [2x2] matrix multiplication and inversion.

**Remark 13.3** Cycles, searches, and symmetries. A few comments about the role of symmetries in actual extraction of cycles. In the  $N$ -disk billiard example, a fundamental domain is a sliver of the  $N$ -disk configuration space delineated by a pair of adjoining symmetry axes. The flow may further be reduced to a return map on a Poincaré surface of section. While in principle any Poincaré surface of section will do, a natural choice in the present context are crossings of symmetry axes, see example 7.7. In actual numerical integrations only the last crossing of a symmetry line needs to be determined. The cycle is run in global coordinates and the group elements associated with the crossings of symmetry lines are recorded; integration is terminated when the orbit closes in the fundamental domain. Periodic orbits with non-trivial symmetry subgroups are particularly easy to find since their points lie on crossings of symmetry lines, see example 7.7.

**Remark 13.4** Newton gone wild. Skowronek and Gora [13.24] offer an interesting discussion of Newton iterations gone wild while searching for roots of polynomials as simple as  $x^2 + 1 = 0$ .

**Remark 13.5** Symmetries of the symbol square. For a discussion of symmetry lines see refs. [7.5, 7.6, 13.6, 7.7, 7.8]. It is an open question (see remark 21.2) as to how time reversal symmetry can be exploited for reduction of cycle expansions of chapter 20. For example, the fundamental domain symbolic dynamics for reflection symmetric systems is discussed in some detail in sect. 21.5, but how does one recode from time-reversal symmetric symbol sequences to desymmetrized 1/2 state space symbols?

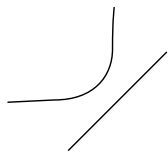
Exercises

- 13.1. **Cycles of the Ulam map.** Test your cycle-searching routines by computing a bunch of short cycles and their stabilities for the Ulam map  $f(x) = 4x(1 - x)$ .
- 13.2. **Cycles stabilities for the Ulam map (exact).** In exercise 13.1 you should have observed that the numerical results for the cycle Floquet multipliers (4.46) are exceptionally simple: the Floquet multiplier of the  $x_0 = 0$  fixed point is 4, while the eigenvalue of any other  $n$ -cycle is  $\pm 2^n$ . Prove this. (Hint: the Ulam map can be conjugated to the tent map (11.4). This problem is perhaps too hard, but give it a try - the answer is in many introductory books on nonlinear dynamics.)

- 13.3. **Stability of billiard cycles.** Compute the stabilities of few simple cycles:

- (a) A simple scattering billiard is the two-disk billiard. It consists of a disk of radius one centered at the origin and another disk of unit radius located at distance  $L + 2$ . Find all periodic orbits for this system and compute their stabilities. (You might have done this already in exercise 1.2; at least now you will be able to see where you went wrong when you knew nothing about cycles and their extraction.)

- (b) Find all periodic orbits and their stabilities for a billiard ball bouncing between the diagonal  $y = x$  and one of the hyperbola branches  $y = -1/x$ .



- 13.4. **Cycle stability.** Add to the pinball simulator of exercise 8.1 a routine that evaluates the expanding eigenvalue for a given cycle.
- 13.5. **Pinball cycles.** Determine the stability and length of all fundamental domain prime cycles of the binary symbol string lengths up to 5 (or longer) for  $R : a = 6$  3-disk pinball.
- 13.6. **Newton-Raphson method.** Implement the Newton-Raphson method in 2 - dimensional and apply it to the determination of pinball cycles.

- 13.7. **Fundamental domain fixed points.** Use the formula (8.11) for billiard Jacobian matrix to compute the periods  $T_p$  and the expanding eigenvalues  $\Lambda_p$  of the fundamental domain  $\bar{0}$  (the 2-cycle of the complete 3-disk space) and  $\bar{1}$  (the 3-cycle of the complete 3-disk space) fixed points:

$$\begin{array}{c|cc} & T_p & \Lambda_p \\ \hline \bar{0}: & R - 2 & R - 1 + R\sqrt{1 - 2/R} \\ \bar{1}: & R - \sqrt{3} & -\frac{2R}{\sqrt{3}} + 1 - \frac{2R}{\sqrt{3}}\sqrt{1 - \sqrt{3}/R} \end{array} \quad (13.24)$$

We have set the disk radius to  $a = 1$ .

- 13.8. **Fundamental domain 2-cycle.** Verify that for the  $\bar{10}$ -cycle the cycle length and the trace of the Jacobian matrix are given by

$$\begin{aligned} L_{10} &= 2\sqrt{R^2 - \sqrt{3}R + 1} - 2, \\ \text{tr } \mathbf{J}_{10} &= \Lambda_{10} + 1/\Lambda_{10} \\ &= 2L_{10} + 2 + \frac{1}{2} \frac{L_{10}(L_{10} + 2)^2}{\sqrt{3}R/2 - 1}. \end{aligned} \quad (13.25)$$

The  $\bar{10}$ -cycle is drawn in figure 12.12. The unstable eigenvalue  $\Lambda_{10}$  follows from (7.30).

- 13.9. **A test of your pinball simulator:  $\bar{10}$ -cycle.** Test your exercise 8.3 pinball simulator stability evaluation by checking numerically the exact analytic  $\bar{10}$ -cycle stability formula (13.25).

- 13.10. **Rössler flow cycles.** (continuation of exercise 4.4) Determine all cycles for the Rössler flow (2.17), as well as their stabilities, up to

- (a) 3 Poincaré section returns  
 (b) (optional) 5 Poincaré section returns (Hint: implement (13.14), the multipoint shooting methods for flows; you can cross-check your shortest cycles against the ones listed in the table.)

**Table:** The Rössler flow (2.17): The itinerary  $p$ , a periodic point  $x_p = (0, y_p, z_p)$  and the expanding eigenvalue  $\Lambda_p$  for all cycles up to topological length 7. (J. Mathiesen, G. Simon, A. Basu)

| $n_p$ | $p$     | $y_p$    | $z_p$    | $\Lambda_p$ |
|-------|---------|----------|----------|-------------|
| 1     | 1       | 6.091768 | 1.299732 | -2.403953   |
| 2     | 01      | 3.915804 | 3.692833 | -3.512007   |
| 3     | 001     | 2.278281 | 7.416481 | -2.341923   |
|       | 011     | 2.932877 | 5.670806 | 5.344908    |
| 4     | 0111    | 3.466759 | 4.506218 | -16.69674   |
| 5     | 01011   | 4.162799 | 3.303903 | -23.19958   |
|       | 01111   | 3.278914 | 4.890452 | 36.88633    |
| 6     | 001011  | 2.122094 | 7.886173 | -6.857665   |
|       | 010111  | 4.059211 | 3.462266 | 61.64909    |
|       | 011111  | 3.361494 | 4.718206 | -92.08255   |
| 7     | 0101011 | 3.842769 | 3.815494 | 77.76110    |
|       | 0110111 | 3.025957 | 5.451444 | -95.18388   |
|       | 0101111 | 4.102256 | 3.395644 | -142.2380   |
|       | 0111111 | 3.327986 | 4.787463 | 218.0284    |

- 13.11. **Cycle stability, helium.** Add to the helium integrator of exercise 2.10 a routine that evaluates the expanding eigenvalue for a given cycle.

- 13.12. **Collinear helium cycles.** Determine the stability and length of all fundamental domain prime cycles up to symbol sequence length 5 or longer for collinear helium of figure 7.2.

- 13.13. **Uniqueness of unstable cycles\*\*\*.** Prove that there exists only one 3-disk prime cycle for a given finite admissible prime cycle symbol string. Hints: look at the Poincaré maps; can you show that there is exponential contraction to a unique periodic point with a given itinerary? Exercise 29.1 might be helpful in this effort.

- 13.14. **Inverse iteration method for a Hénon repeller.**

**Table:** All periodic orbits up to 6 bounces for the Hamiltonian Hénon mapping (13.26) with  $a = 6$ . Listed are the cycle itinerary, its expanding eigenvalue  $\Lambda_p$ , and its "center of mass." The "center of mass" is listed because it turns out that it is often a simple rational or a quadratic irrational.

| $p$    | $\Lambda_p$               | $\sum x_{p,i}$ |
|--------|---------------------------|----------------|
| 0      | 0.715168×10 <sup>1</sup>  | -0.607625      |
| 1      | -0.295285×10 <sup>1</sup> | 0.274292       |
| 10     | -0.989898×10 <sup>1</sup> | 0.333333       |
| 100    | -0.131907×10 <sup>3</sup> | -0.206011      |
| 110    | 0.558970×10 <sup>2</sup>  | 0.539345       |
| 1000   | -0.104430×10 <sup>4</sup> | -0.816497      |
| 1100   | 0.577998×10 <sup>4</sup>  | 0.000000       |
| 1110   | -0.103688×10 <sup>3</sup> | 0.816497       |
| 10000  | -0.760653×10 <sup>4</sup> | -1.426032      |
| 11000  | 0.444552×10 <sup>4</sup>  | -0.606654      |
| 10100  | 0.770202×10 <sup>3</sup>  | 0.151375       |
| 11100  | -0.710688×10 <sup>3</sup> | 0.248463       |
| 11010  | -0.589499×10 <sup>3</sup> | 0.870695       |
| 11110  | 0.390994×10 <sup>3</sup>  | 1.095485       |
| 100000 | -0.545745×10 <sup>5</sup> | -2.034134      |
| 110000 | 0.322221×10 <sup>5</sup>  | -1.215250      |
| 101000 | 0.513762×10 <sup>4</sup>  | -0.450662      |
| 111000 | -0.478461×10 <sup>4</sup> | -0.366025      |
| 110100 | -0.639400×10 <sup>4</sup> | 0.333333       |
| 101100 | -0.639400×10 <sup>4</sup> | 0.333333       |
| 111100 | 0.390194×10 <sup>4</sup>  | 0.548583       |
| 111010 | 0.109491×10 <sup>4</sup>  | 1.151463       |
| 111110 | -0.104338×10 <sup>4</sup> | 1.366025       |

Consider the Hénon map (3.17) for the area-preserving ("Hamiltonian") parameter value  $b = -1$ . The coordinates of a periodic orbit of length  $n_p$  satisfy the equation

$$x_{p,i+1} + x_{p,i-1} = 1 - ax_{p,i}^2, \quad i = 1, \dots, n_p, \quad (13.26)$$

with the periodic boundary condition  $x_{p,0} = x_{p,n_p}$ . Verify that the itineraries and the stabilities of the short periodic orbits for the Hénon repeller (13.26) at  $a = 6$  are as listed above.

**Hint:** you can use any cycle-searching routine you wish, but for the complete repeller case (all binary sequences are realized), the cycles can be evaluated simply by inverse iteration, using the inverse of (13.26)

$$x''_{p,i} = S_{p,i} \sqrt{\frac{1 - x'_{p,i+1} - x'_{p,i-1}}{a}}, \quad i = 1, \dots, n_p.$$

Here  $S_{p,i}$  are the signs of the corresponding periodic point coordinates,  $S_{p,i} = x_{p,i}/|x_{p,i}|$ . (G. Vattay)

- 13.15. **Ulam map periodic points.** (continued from exercise 11.8)

- (a) compute the five periodic points of cycle  $\bar{10011}$  for the Ulam map (11.5)  $f(x) = 4x(1 - x)$  using your Newton or other routine.  
 (b) compute the five periodic points of cycle  $\bar{10000}$   
 (c) plot the above two cycles on the graph of the Ulam map, verify that their topological ordering is as in the 'canonical' full tent map exercise 11.8.

- (d) (optional) This works only for the Ulam map; compute periodic points by conjugating the full tent map periodic points of exercise 11.8 using exercise 6.4.

- 13.16. **Newton setups for flows.**

- (a) We have formulated three Newton setups for flows: the 'local' setup (13.11), the 'hyperplane' setup (13.14), and the 'global' setup (13.20). Derive (13.20) and verify that if the surface of section is a hyperplane, it reduces to (13.14). (Hint: it is not inconceivable that (13.14) is wrong as it stands.)

- (b) (optional) Derive (13.22), the Newton setup for Hamiltonian flows.

- 13.17. **"Center of mass" puzzle\*\*.** Why is the "center of mass," tabulated in exercise 13.14, often a rational number?

## References

- [13.1] D. Auerbach, P. Cvitanović, J.-P. Eckmann, G.H. Gunaratne and I. Procaccia, *Phys. Rev. Lett.* **58**, 2387 (1987).
- [13.2] M. Baranger and K.T.R. Davies *Ann. Physics* **177**, 330 (1987).
- [13.3] B.D. Mestel and I. Percival, *Physica D* **24**, 172 (1987); Q. Chen, J.D. Meiss and I. Percival, *Physica D* **29**, 143 (1987).
- [13.4] find Helleman et all Fourier series methods
- [13.5] J.M. Greene, *J. Math. Phys.* **20**, 1183 (1979)
- [13.6] P.H. Richter, H.-J. Scholz and A. Wittek, "A breathing chaos," *Nonlinearity* **1**, 45 (1990).
- [13.7] H.E. Nusse and J. Yorke, "A procedure for finding numerical trajectories on chaotic saddles" *Physica D* **36**, 137 (1989).
- [13.8] D.P. Lathrop and E.J. Kostelich, "Characterization of an experimental strange attractor by periodic orbits" *Phys. Rev. A* **40**, 4028 (1989).
- [13.9] T. E. Huston, K.T.R. Davies and M. Baranger *Chaos* **2**, 215 (1991).
- [13.10] M. Brack, R. K. Bhaduri, J. Law and M. V. N. Murthy, *Phys. Rev. Lett.* **70**, 568 (1993).
- [13.11] J. J. Crofts and R. L. Davidchack, "Efficient detection of periodic orbits in chaotic systems by stabilising transformations;" [arXiv:nlin.CD/0502013](https://arxiv.org/abs/nlin.CD/0502013).
- [13.12] J. J. Crofts and R. L. Davidchack, "On the use of stabilizing transformations for detecting unstable periodic orbits in high-dimensional flows," *Chaos* **19** (2009).
- [13.13] C. Polymilis, G. Servizi, Ch. Skokos, G. Turchetti, and M. N. Vrahatis, "Locating periodic orbits by Topological Degree theory;" [arXiv:nlin.CD/0211044](https://arxiv.org/abs/nlin.CD/0211044).
- [13.14] B. Doyon and L. J. Dubé, "On Jacobian matrices for flows," *CHAOS* **15**, 013108 (2005).
- [13.15] S.C. Farantos, "Exploring Molecular Vibrational Motions with Periodic Orbits," *Int. Rev. Phys. Chem.* **15**, 345 (1996); [tccc.iesl.forth.gr/~farantos](http://tccc.iesl.forth.gr/~farantos), [tccc.iesl.forth.gr/articles/review/review1.ps.gz](http://tccc.iesl.forth.gr/articles/review/review1.ps.gz).
- [13.16] S.C. Farantos, "POMULT: A Program for Computing Periodic Orbits in Hamiltonian Systems Based on Multiple Shooting Algorithms," *Computer Phys. Comm.* **108**, 240 (1998); [esperia.iesl.forth.gr/~farantos/articles/po\\_cpc/po\\_ccp.ps](http://esperia.iesl.forth.gr/~farantos/articles/po_cpc/po_ccp.ps).
- [13.17] M. Baranger, K.T.R. Davies and J.H. Mahoney, "The calculation of periodic trajectories," *Ann. Phys.* **186**, 95 (1988).
- [13.18] K.T.R. Davies, T.E. Huston and M. Baranger, "Calculations of periodic trajectories for the Henon-Heiles Hamiltonian using the monodromy method," *CHAOS* **2**, 215 (1992).
- [13.19] N.S. Simonović, "Calculations of periodic orbits: The monodromy method and application to regularized systems," *CHAOS* **9**, 854 (1999).
- [13.20] N.S. Simonović, "Calculations of Periodic Orbits for Hamiltonian Systems with Regularizable Singularities," *Few-Body-Systems* **32**, 183 (2003).
- [13.21] Z. Gills, C. Iwata, R. Roy, I.B. Schwartz and I. Triandaf, "Tracking Unstable Steady States: Extending the Stability Regime of a Multimode Laser System," *Phys. Rev. Lett.* **69**, 3169 (1992).
- [13.22] N.J. Balmforth, P. Cvitanović, G.R. Ierley, E.A. Spiegel and G. Vattay, "Advection of vector fields by chaotic flows," *Stochastic Processes in Astrophysics, Annals of New York Academy of Sciences* **706**, 148 (1993); preprint.
- [13.23] A. Endler and J.A.C. Gallas, "Rational reductions of sums of orbital coordinates for a Hamiltonian repeller," (2005).
- [13.24] L. Skowronek and P. F. Gora, "Chaos in Newtonian iterations: Searching for zeros which are not there," *Acta Phys. Polonica B* **38**, 1909 (2007); [arXiv:nlin.CD/0703061](https://arxiv.org/abs/nlin.CD/0703061).